Pediatric Radiology (2020) 50:1810–1829
https://doi.org/10.1007/s00247-020-04768-0

FETAL IMAGING

How to read a fetal magnetic resonance image 101

Ailish C. Coblentz[1] · Sara R. Teixeira[1] · David M. Mirsky[2] · Ann M. Johnson[1] · Tamara Feygin[1] · Teresa Victoria[1]

Received: 21 April 2020 / Revised: 22 May 2020 / Accepted: 1 July 2020 / Published online: 19 November 2020

Abstract
Accurate antenatal diagnosis is essential for planning appropriate pregnancy management and improving perinatal outcomes. The provision of information vital for prognostication is a crucial component of prenatal imaging, and this can be enhanced by the use of fetal MRI. Image acquisition, interpretation and reporting of a fetal MR study can be daunting to the individual who has encountered few or none of these examinations. This article provides the radiology trainee with a general approach to interpreting a fetal MRI. The authors review the added value of prenatal MRI in the overall assessment of fetal wellbeing, discuss MRI protocols and techniques, and review the normal appearance of maternal and fetal anatomy. The paper concludes with a sample template for structured reporting, to serve as a checklist and guideline for reporting radiologists.

Keywords Fetus · Interpretation · Magnetic resonance imaging · Normal anatomy · Obstetrics

Introduction

Accurate antenatal diagnosis is essential in planning appropriate pregnancy management and improving perinatal outcomes. While many prenatally diagnosed conditions can be managed conservatively, others require specialized planning for delivery and early postnatal management, or might be suitable for antenatal surgical intervention [1, 2]. Certain conditions remain universally fatal. Providing information vital for prognostication is a crucial component of prenatal imaging, and this can be enhanced by the use of fetal MRI.

The Society for Pediatric Radiology provides the following indications for fetal MRI: (1) to provide adjuvant information when sonography is unable to clearly define an abnormality and more information is needed, for example in the setting of maternal obesity; (2) when MR-specific information is required to make decisions about care, for example, calculated lung volumes in cases of congenital diaphragmatic hernia; and (3) when a fetus is at significant risk for an abnormality that might be sonographically occult, for example neurologic ischemia following laser ablation for twin–twin transfusion [3].

The optimal timing for performing MRI is dependent on the pathology suspected by sonography. Before 18 weeks, fetal organs are underdeveloped, movement is increased, and certain pathologies might not have developed [4, 5]. Although MRI can be performed at any gestational age, it is typically done after 20 weeks, to improve visualization of the fetal organs [5, 6]. It is judicious to expedite the MRI study when an abnormality is suspected sonographically, particularly in cases where the parents are considering termination.

Fetal MRI interpretation is improved by a multidisciplinary approach, which can include specialists in perinatal imaging, obstetricians and neonatologists. This helps providers in the delivery of care and ensures that parents receive the most accurate information regarding perinatal and long-term outcome.

Interpreting and reporting a fetal MR study might be daunting to the individual who has encountered few or none of these examinations. We provide the radiology trainee with a general approach to interpreting a fetal MRI.

Value of magnetic resonance imaging

While sonography remains the first-line modality in fetal imaging, it has several well-known limitations. Factors including

✉ Teresa Victoria
victoria@email.chop.edu

[1] Radiology Department,
The Children's Hospital of Philadelphia,
34th Street and Civic Center Boulevard,
Philadelphia, PA 10104, USA

[2] Neuroradiology Department,
Children's Hospital of Colorado,
Aurora, CO, USA

oligo- and anhydramnios, anterior placenta, large maternal body habitus, complex malformations, and operator dependence can hamper sonographic assessment [7]. For these reasons, fetal MRI is an increasingly available noninvasive tool that can be used as an adjuvant to ultrasound. Individual fetal structures including the brain, lungs, liver, kidneys and bowel can be distinguished because of the superior soft-tissue contrast resolution of MR [8, 9]. Technical advances have also made it possible to acquire functional imaging and to provide volumetric data [10].

A recent meta-analysis reviewed MRI as compared to sonography in the diagnosis of fetal brain abnormalities. In 80% of cases, the postnatal diagnosis agreed completely with the fetal MRI diagnosis, whereas it matched the neurosonographic diagnosis only 54% of the time [11]. While MRI is particularly useful in the evaluation of central nervous system anomalies, it can also serve as an adjunct to US in assessment of the fetal thorax and abdomen [8]. Additional value has been illustrated in the context of assessing anomalies under evaluation for possible fetal therapy [12], and in characterizing placental abnormalities [13]. The large field of view, multiplanar capabilities, and utility in demonstrating an abnormality within the context of the entire fetal body allow fetal MRI to provide an effective visual roadmap for surgeons and obstetricians alike.

Magnetic resonance imaging protocols and techniques

Patient preparation is paramount to acquiring high-quality images. Our institution allows the mother to be accompanied in the MR room. This can help alleviate anxiety and improve the likelihood of a completed scan. When possible, women are imaged in the supine position, with a pillow under the knees and an empty bladder. Later in gestation, the MR scan can be performed with the woman in a left oblique or lateral decubitus position, to reduce compression on the inferior vena cava. Fetal movement presents a distinct challenge to acquiring diagnostic-quality images. The development of ultrafast MR sequences has eliminated the need for maternal or fetal sedation. In an effort to further reduce motion, some centers advocate for maternal fasting or prohibit caffeine intake in advance of the scan. However, the data suggest that diet and meal timing do not play a substantial role in limiting fetal movement [14]. Before scanning, the prior US images should be reviewed to tailor the MR examination to the region of interest (ROI).

Our MRI protocol is performed on a 1.5-tesla (T) or 3-T scanner. The sequences and purpose for each are summarized in Table 1. The first sequences acquired are the localizers. The localizer sequences are obtained in the three orthogonal planes with respect to the mother using fast T2-weighted sequences. We use 6- to 8-mm single-shot fast spin-echo (SSFSE) T2-weighted slices with a 1–2-mm gap and a large field of view (320–400 mm). The localizers are used for initial visualization, to optimize the signal intensity for the subsequent diagnostic sequences, and to ensure that the fetal ROI is in the center of the coil [9]. The fetus is a moving target and scanning is a dynamic process, with each acquisition serving as a scout image for the following sequence. Coil re-adjustments might be required throughout scanning to ensure that the fetus remains at the isocenter. At our center, coronal and sagittal T2-W single-shot turbo spin-echo (SSTSE) sequences with respect to mom are acquired next. These are used to establish fetal situs and to assess the visualized maternal abdomen and pelvis. In particular, close attention should be paid to the cervix (Fig. 1). After obtaining an overview of the pregnancy, our attention is turned to evaluation of the fetus, which employs a variety of fast MRI sequences in multiple planes.

Fluid-sensitive single-shot turbo spin echo (SSTSE)

Fluid-sensitive single-shot turbo spin-echo (SSTSE) sequences are the workhorse of fetal MR imaging. Triplanar images are acquired, angulated to the planes of the fetus. The ultrafast T2-weighted sequences provide high-resolution anatomical imaging. The single-slice acquisition means that episodes of fetal motion usually affect the particular slice being obtained when the motion

Table 1 Sample fetal magnetic resonance imaging (MRI) protocol

MR sequence	Purpose
Localizers	Initial fetal visualization/ensure ROI centered in coil
Coronal & sagittal T2-W SSTSE with respect to mom	Fetal situs/maternal assessment
Multiplanar T2-W SSTSE (fetus)	Global overview of the fetus/anatomical detail of ROI
Multiplanar SSFP (fetus)	Heart/vessels/overall anatomy
EPI (fetus)	Musculoskeletal/liver/calcifications/blood products (especially in the brain)
T1-weighted images (fetus)	Meconium/liver/thyroid/hemorrhage/fat/myelination

EPI echoplanar imaging, *ROI* region of interest, *SSFP* steady-state free precession, *SSTSE* single-shot turbo spin echo

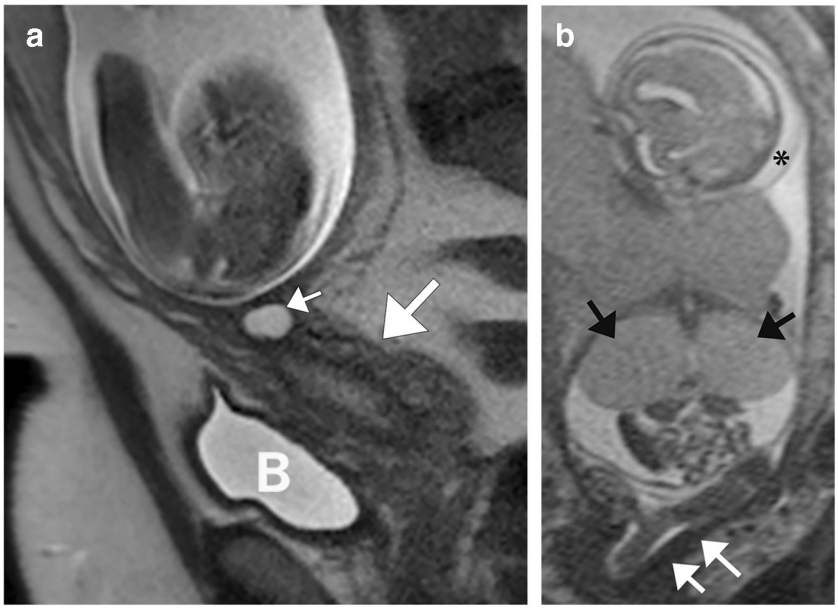

Fig. 1 MR evaluation of the cervix. **a** Sagittal single-shot turbo spin-echo (SSTSE) MR image through the cervix in a 33-year-old gravid woman carrying a fetus with omphalocele (not shown). Note the normal layers of the cervix (*large arrow*) and the incidental presence of a nabothian cyst (*small arrow*). *B* maternal bladder. **b** Coronal SSTSE image of an 18-week fetus with congenital high-airway obstruction syndrome (CHAOS). In this case the fetal feet are in the open cervix (*white arrows*) in a case of abortion in progress. The fetus has CHAOS, depicted in the partially imaged, markedly hyper-expanded T2-hyperintense lungs (*black arrows*) and the presence of ascites and skin edema (*asterisk*)

occurred [15]. Although particular attention should be paid to the area of concern identified by US, the T2-weighted single-shot images provide an essential global overview of the fetus. It is important to remember that it is not uncommon to discover additional anomalies after an initial working diagnosis of an isolated pathology [12].

Steady-state free precession (SSFP)

Steady state free precession (SSFP) sequences are used in conjunction with T2-weighted SSTSE to provide a second perspective of the fetal anatomy. The anatomical resolution is superior to that of SSTSE at 3-T magnet strength, although this is not the case at 1.5 T [16]. Contrary to T2-weighted SSTSE, which is a black-blood sequence, the bright-blood of SSFP renders it a useful sequence in assessing the fetal heart and vascular structures [17]. Three-dimensional (3-D) SSFP images can provide supplementary information where there is a specific question regarding the exact anatomical site of a detected abnormality, or provide reconstructions that are helpful in preparing parents and clinicians (Fig. 2). Cine SSFP sequences can be helpful in the dynamic assessment of moving structures, including fetal swallowing in a fetus with a large head and neck teratoma, or in assessing peristalsis in a fetus with dilated bowel. In cases of tracheoesophageal fistula, cine images in the sagittal plane are particularly helpful in evaluating for the presence of an esophageal pouch because it can appear transiently with intermittent fetal swallows.

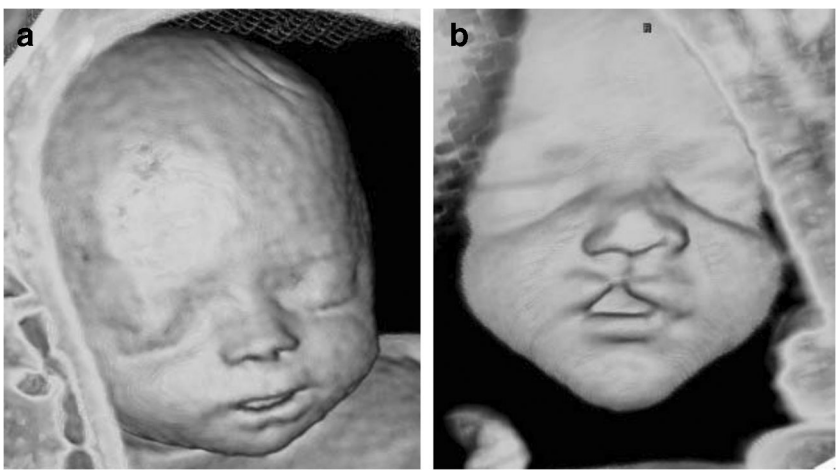

Fig. 2 The fetal face. **a, b** Anterior volume-rendered images obtained from a 3-D steady-state free precession sequence demonstrate the face of a normal fetus (**a**) and that of a fetus with a cleft lip (**b**). Images courtesy of Monica Epelman, MD

Echoplanar imaging (EPI)

Echoplanar imaging (EPI) is subject to degradation by considerable magnetic susceptibility artifact, particularly from bowel content in the gravid patient [18]. However, this susceptibility can be used to the radiologist's advantage when assessing for calcification and intracranial blood products. The liver is well visualized by EPI, appearing much darker than the surrounding abdominal organs and adjacent lungs. This is helpful in cases of congenital diaphragmatic hernia, when EPI can best show the presence of liver herniation, an important prognostic factor [19]. The relative hypointensity of bones and muscles with EPI is useful for evaluating the musculoskeletal system (Fig. 3).

T1-weighted images

T1-weighted images can be obtained by either conventional spin-echo or breath-hold spoiled gradient echo sequences [20]. The T1-weighted gradient echo images are more prone to motion artifacts, as is the case of most gradient echo sequences; however, breath-holding greatly improves image quality (Fig. 3). T1-weighted images are of particular value for evaluating the fetal abdomen because of the intrinsic T1 hyperintensity of the liver and meconium within the bowel. Hemorrhage, fat, calcifications and the normal iodine-containing thyroid are also T1 hyperintense, and most are readily identified with these sequences.

Additional fetal magnetic resonance imaging techniques

Additional fetal MRI techniques that can add value in fetal assessment include diffusion-weighted imaging (DWI), diffusion tensor imaging (DTI) and MR spectroscopy [9, 15]. In the assessment of the fetal brain, newer DWI sequences have contributed to the increased accuracy of prenatal detection and timing of fetal stroke and hypoxic–ischemic injury (Fig. 3). DWI has also been used for better visualization of hemorrhage, cysts and fetal tumors [21]. DTI has the potential to reveal neuro-connectivity and is capable of characterizing

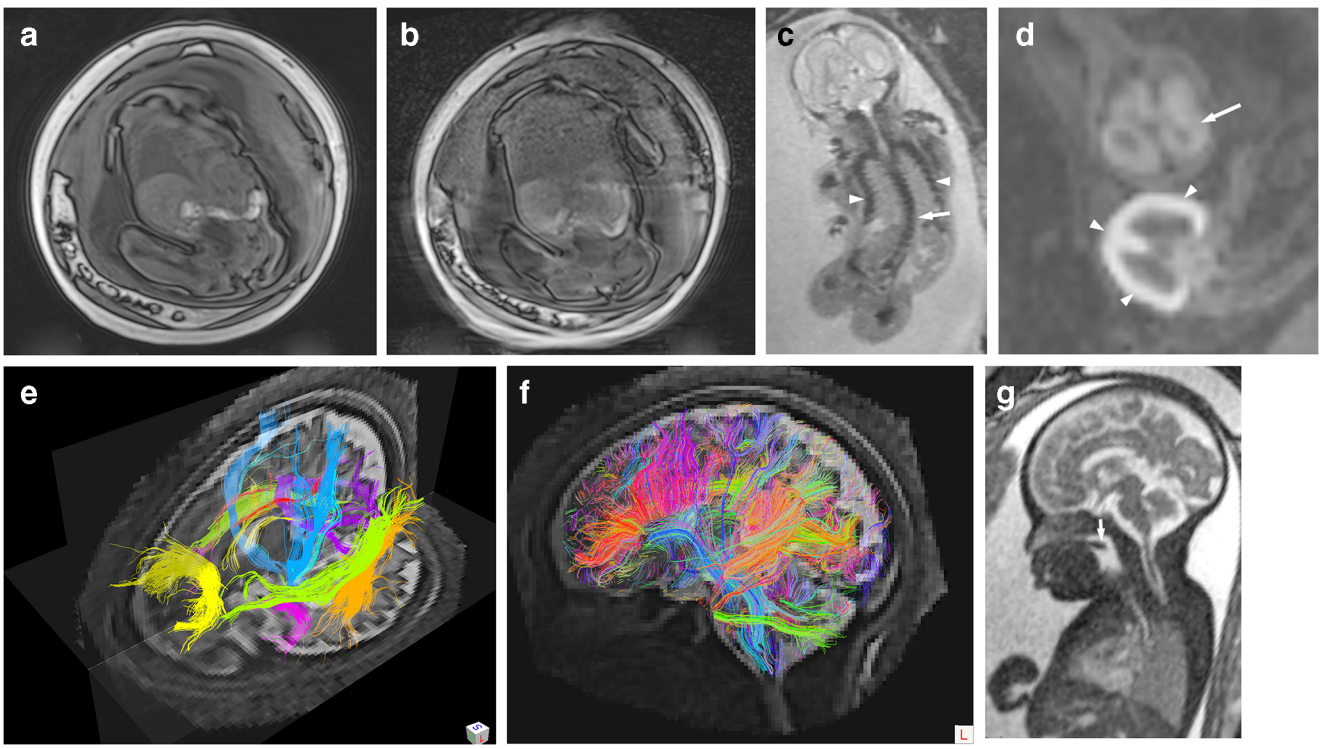

Fig. 3 Fetal MR sequences. **a, b** T1-weighted images are fundamental in evaluating the fetus. The thyroid, liver and meconium are T1 hyperintense in the normal fetus. T1-weighting also aids in evaluating for hemorrhage. Acquiring T1-W images benefits from maternal breath-hold, as demonstrated in these coronal images of the same 34-week fetus with (**a**) and without (**b**) breath-hold. Note the sharper borders and anatomy seen with breath-holding. **c** Coronal echoplanar imaging (EPI) shows a 22-week fetus with congenital musculoskeletal scoliosis (*arrow*) and bell-shape thorax (*arrowheads*). **d** Axial diffusion-weighted imaging (DWI) of the brains of these 19-week twins with twin–twin transfusion syndrome (TTTS) demonstrates restricted diffusion of the entire brain, indicative of global hypoxic–ischemic injury, in one twin (*arrowheads*), and normal diffusion pattern in the other twin (*arrow*). **e, f** Three-dimensional (**e**) and two-dimensional (**f**) sagittal reconstructed diffusion tensor images (DTI) in a 36-week fetus beautifully demonstrate the development of neural connectivity and fiber bundles of the brain (images courtesy of Camilo Jaimes Cobos, MD, and Fedel Machado, MD). **g** Sagittal steady-state free precession (SSFP) cine image shows elevation of the soft palate (*arrow*) during normal swallowing of amniotic fluid in this 32-week fetus

microstructural development and demonstrating fiber bundles [21] (Fig. 3). MR spectroscopy has been applied in the assessment of fetal brain metabolism, for example in the setting of congenital heart disease [22].

In addition, technical advancements in fetal cardiac imaging might eventually allow for diagnostic cine imaging and 4-D volumetric reconstructions [23]. Real-time cine MRI is being used with increasing frequency for assessing numerous functional tasks of the fetal organs/systems. This dynamic 2-D fast imaging technique with steady-state acquisition is based on the organization of images in a sequential loop, resulting in observation of a real-time movie. It can provide a high-quality assessment and recording of the entire process of amniotic fluid transmission from the fetal mouth to the trachea and esophagus (Fig. 3); the significance this information for prenatal counseling and delivery planning cannot be overestimated, especially in fetuses with head and neck pathology.

Last, new and promising techniques to assess the fetal brain, placenta and other organs beyond morphology include intravoxel incoherent motion [24], which can yield information about perfusion, and macromolecular proton fraction [25], although detailed discussion of these technique is beyond the scope of this paper.

Gadolinium contrast has been shown to cross the placenta, likely without adverse effects on the fetus [26]. However, it might remain in the fetal circulation for a prolonged period because of recirculation through the amniotic fluid the fetus swallows [12, 27]. Gadolinium-based agents are not presently approved by the U.S. Food and Drug Administration for use in pregnancy, and are not recommended for use in fetal MR [9].

At most institutions, fetal MR studies are performed as monitored examinations. A pediatric radiologist reviews the images as they are acquired, adjusting the imaging planes and sequences as required, to answer the clinical question. Ideally, it is desirable to scan the pregnant woman with US immediately prior to the MRI. This is to check fetal position and thoroughly characterize the pathology in question.

Basic approach to fetal magnetic resonance interpretation

As in all branches of diagnostic imaging, interpretation of a fetal MRI requires the radiologist to adopt a structured approach and to follow a diagnostic checklist. Knowledge of what constitutes normal at different gestational ages is imperative to identify abnormal development. The gestational age is calculated based on the first day of the mother's last menstrual period and adjusted based on US measurements. This should be kept in mind when going through the study and should frame the way in which findings are interpreted. Next we provide a basic systematic approach that can be used by radiologists learning to report fetal MRI studies.

Extrafetal findings

Maternal evaluation

The wide-field-of-view images provide an opportunity to search for any unexpected maternal findings. When possible, both maternal ovaries should be identified to exclude any pathology (Fig. 4). Incidental abnormalities noted in the other maternal structures, including the kidneys, bones and other viscera, should be reported [28]. It should be noted that mild hydronephrosis (particularly on the right side) is present in 90% of pregnancies and should be considered a normal phenomenon [29].

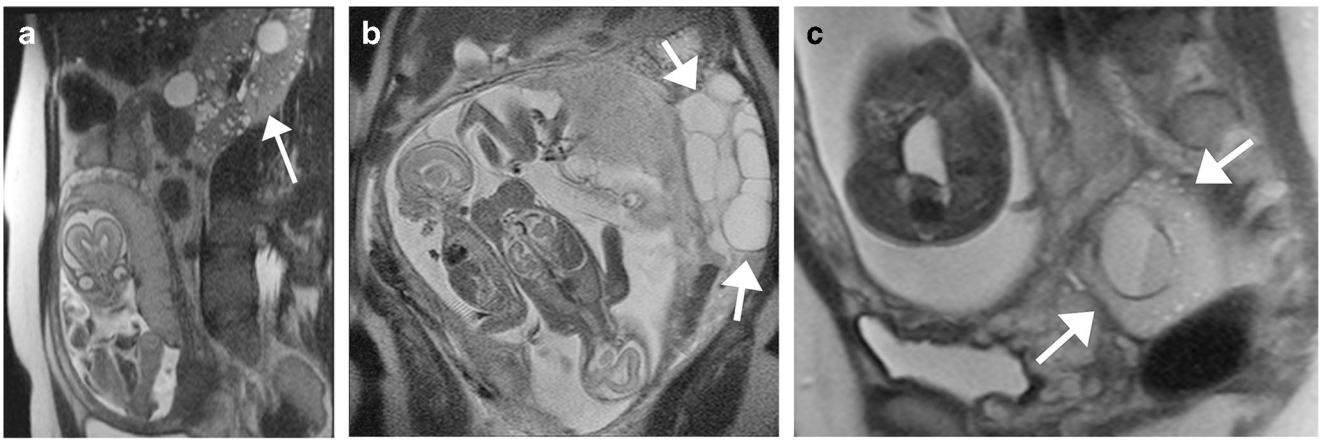

Fig. 4 Abnormal maternal findings found at fetal MRI. Attention must always be paid to the maternal organs in a fetal MR examination. **a** Imaging in a 19-week fetus with neck mass (not shown). The maternal kidney shown in this single-shot turbo spin-echo (SSTSE) sagittal image demonstrates numerous parenchymal cysts (*arrows*) in this 31-year-old woman with an, until then, unknown diagnosis of polycystic kidney disease. **b** Imaging in a 21-week triplet gestation shown on coronal SSTSE with respect to the maternal axis in a 35-year-old woman. The maternal ovaries are enlarged and replaced by cysts in this overstimulated ovary (*arrows*). **c** In a 25-week gestation, sagittal (with respect to the maternal axis) SSTSE MR image in the 33-year-old gravid woman demonstrates a maternal dermoid (*arrows*)

Uterus

The gravid uterus is wider at the fundus and its shape has been likened to an upside-down pear. It should have a smooth contour without focal nodularity. The thickness of the myometrium varies throughout pregnancy, becoming progressively thinner at more advanced stages. It initially has a trilayered "oreo-cookie" appearance, with a hypervascular hyperintense core. The three layers eventually stretch out into a thin solitary T2-hypointense layer. Myometrial contractions might be observed as a normal finding and should not be mistaken for fibroids or placental abnormalities (Fig. 5). These contractions appear as transient episodes of rounded focal uterine thickening that is T2 hypointense. They should be transitory and resolve or vary throughout the study [28, 30]. Prior uterine interventions can result in the formation of synechia or uterine adhesions (Fig. 6). These shelves of avascular fibrous scar tissue most often form between the anterior and posterior walls of the uterus. Adhesive bands should be distinguished from amniotic bands, which result from rupture of the amnion. This leads to the development of strands of tissue, or so-called amniotic band syndrome. Entrapment of fetal parts by these tissue strands can result in compromised blood supply, with resultant edema in the distal soft tissues. Left untreated, amputation can result. While the bands themselves are often thin and imperceptible by MR, their presence can sometimes be inferred by their effect on the fetus [28]. The cervix should remain long and closed throughout pregnancy. Measured in the sagittal plane, 25 mm is the usual lower limit for cervical length [28], although this varies with gestational age and number of previous gestations. The signal of the cervix is also trilaminate. The innermost central zone is markedly T2 hyperintense, relating to the presence of mucus within the cervical plug [30]. The surrounding stroma is formed by a T2-hypointense inner layer and an intermediate signal outer layer. Loss of differentiation between these layers is also associated with loss in cervical length and can be a harbinger of spontaneous preterm delivery [28].

Placenta

The placenta is usually located along the anterior or posterior wall of the uterus. Placental size is expressed in terms of thickness and should measure between 2 cm and 4 cm at the midportion. Systemic vascular conditions causing microinfarctions can result in placental thinning. Placental thickening (>4 cm, depending on GA) occurs with antepartum infections, fetal hydrops, maternal diabetes and anemia [30, 31]. The signal characteristics of the placenta depend on the MR pulse sequence. With T2-W SSTSE imaging, the most commonly utilized sequence in fetal imaging, the second-trimester placenta is of intermediate signal and is typically slightly hyper- or isointense to the adjacent myometrium (Fig. 7). A similar appearance is demonstrated with SSFP and T1-weighted imaging. The placenta has a homogeneous appearance during the first trimester and becomes progressively heterogeneous as it matures. Particularly in the third trimester, high-signal round structures might be discerned on fluid-sensitive sequences, representing the placental cotyledons. When placental hematoma is suspected, DWI is excellent for demonstrating blood breakdown products because of susceptibility effects [32].

The placental surface is smooth earlier in gestation, later developing gentle lobulations along its fetal surface [30]. As the myometrium thins throughout pregnancy, it might appear to blend into the placenta, rendering it difficult to delineate the interface between the two structures. This makes diagnosing placental adhesive disorders challenging. The imaging findings of disordered placentation have been described and are beyond the scope of this review [33].

The placenta is usually discoid, but variants include bilobed, succenturiate and circumvallate morphologies. A succenturiate placenta has an accessory lobule that is separate from the main placental body. When the fetal membranes (chorion and amnion) double back around the placental edge, giving a rolled appearance,

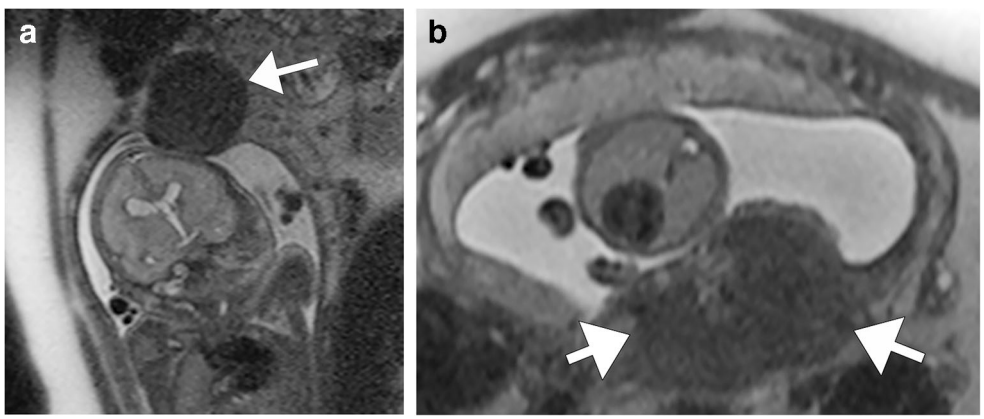

Fig. 5 Uterine masses and pseudomasses. **a, b** Sagittal single-shot turbo spin-echo (SSTSE) images of the maternal pelvis demonstrate a fibroid (*arrow* in **a**) in a 25-year-old pregnant woman, vs. the uterine contraction (*arrows* in **b**) as shown on this axial SSTSE image of the pelvis in a 27-year-old woman. Contractions tend to change shape during the study, whereas fibroids do not

Fig. 6 Amniotic bands. **a** Sagittal single-shot turbo spin-echo (SSTSE) MR image in a 25-week fetus shows an amniotic band constricting the mid-lower extremity, with marked soft-tissue swelling distal to the constricting band (*arrows*) and resulting vascular compromise. The band was fetoscopically lysed, resulting in return of vascular flow to the lower extremity. **b** Coronal MR image with respect to the maternal uterus in this 21-week gestation fetus shows incidental synechia (*arrow*) crossing the gravid uterus. A synechia should not constrict fetal parts

the placenta is termed circumvallate. Placenta previa refers to an abnormally low position of the placenta in the lower uterine segment. Normally, the inferior margin of the placenta should be at least 2 cm from the internal cervical os. Placenta previa should not be diagnosed before 15 weeks of gestation because the position might change throughout pregnancy. As such, placental position should be re-evaluated later in gestation to confirm location prior to delivery. The placental position is better defined in a sagittal MR sequence orientated to the plane of the cervix.

Umbilical cord

The umbilical cord normally inserts centrally within the placenta. When the cord inserts less than 1 cm from the placental edge, it is considered marginal (or eccentric) insertion. A velamentous insertion is when the cord inserts on the chorioamniotic membranes instead of onto the body of the placenta. The cord has an average length of 55 cm, and typically coils counter-clockwise [28]. A lack of coiling and a short cord might be associated with congenital abnormalities and fetal immobility, respectively, as is seen in cases of limb–body wall complex [34]. The normal cord comprises three vessels (two arteries and one vein), best appreciated in the transverse plane (Fig. 8). Because of the fast flow within the vessels, the blood appears black on T2-W SSTSE and white on SSFP images [28]. The presence of a two-vessel cord (one artery and one vein) should prompt a search for associated congenital anomalies, most often involving the cardiovascular and genitourinary systems [28, 35]. The presence of a three-vessel cord is confirmed by ensuring an artery is present on both sides of the fetal urinary bladder. A nuchal cord is present when the umbilical cord wraps around the fetal neck. Single nuchal cord loops are a relatively common and often without clinical significance. Conversely, multiple (more than two) loops around the neck could cause harm to the fetus [36]. Umbilical co rd cysts are usually pseudocysts (also known as Wharton jelly cysts), and might be associated with congenital anomalies or aneuploidy [37]. True umbilical cord cysts are less common.

Amniotic fluid

Amniotic fluid provides a favorable environment for fetal development. Its main sources are fetal urine production, fetal lung fluid, and nasal/oral secretions [38, 39]. Whilst absolute amniotic fluid volume appears to peak at about 30 weeks of gestational age [39], the ratio of fluid-to-fetus occupying the uterus trends differently. Earlier in gestation, the relatively small and mobile fetus should be bathed in a pool of fluid. As the fetus enlarges throughout pregnancy, the relative proportion of the uterus occupied by fluid vs. fetus decreases. Particularly in the third trimester, the fetus subjectively appears to be surrounded by far less fluid. Abnormal amniotic fluid volume might be idiopathic or reflect an underlying fetal issue. Reduced amniotic fluid volume (oligohydramnios) might be associated with genitourinary abnormalities, or membrane rupture. Increased amniotic fluid volume (polyhydramnios) might be associated with maternal diabetes, fetal hydrops, twin pregnancies or fetal structural anomalies. This includes abnormalities linked with impaired swallowing, seen in certain neurologic disorders, or secondary to gastrointestinal obstruction, as in duodenal atresia [39]. Normal amniotic fluid is homogeneously T2 hyperintense and T1 hypointense. At our institution we do not specifically measure the amniotic fluid volume. We instead rely on a subjective assessment of whether the amount appears adequate for the gestational age, and correlates with ultrasound values. Recently, we have employed a post-processing technique that measures the absolute MR amniotic fluid volume within the entire gravid uterus [40]. We have yet to construct MR normograms for what constitutes normal at each gestational age.

Fetal position and situs

Having completed our examination of the maternal and extrafetal structures, we can now focus on the fetus. The first step in

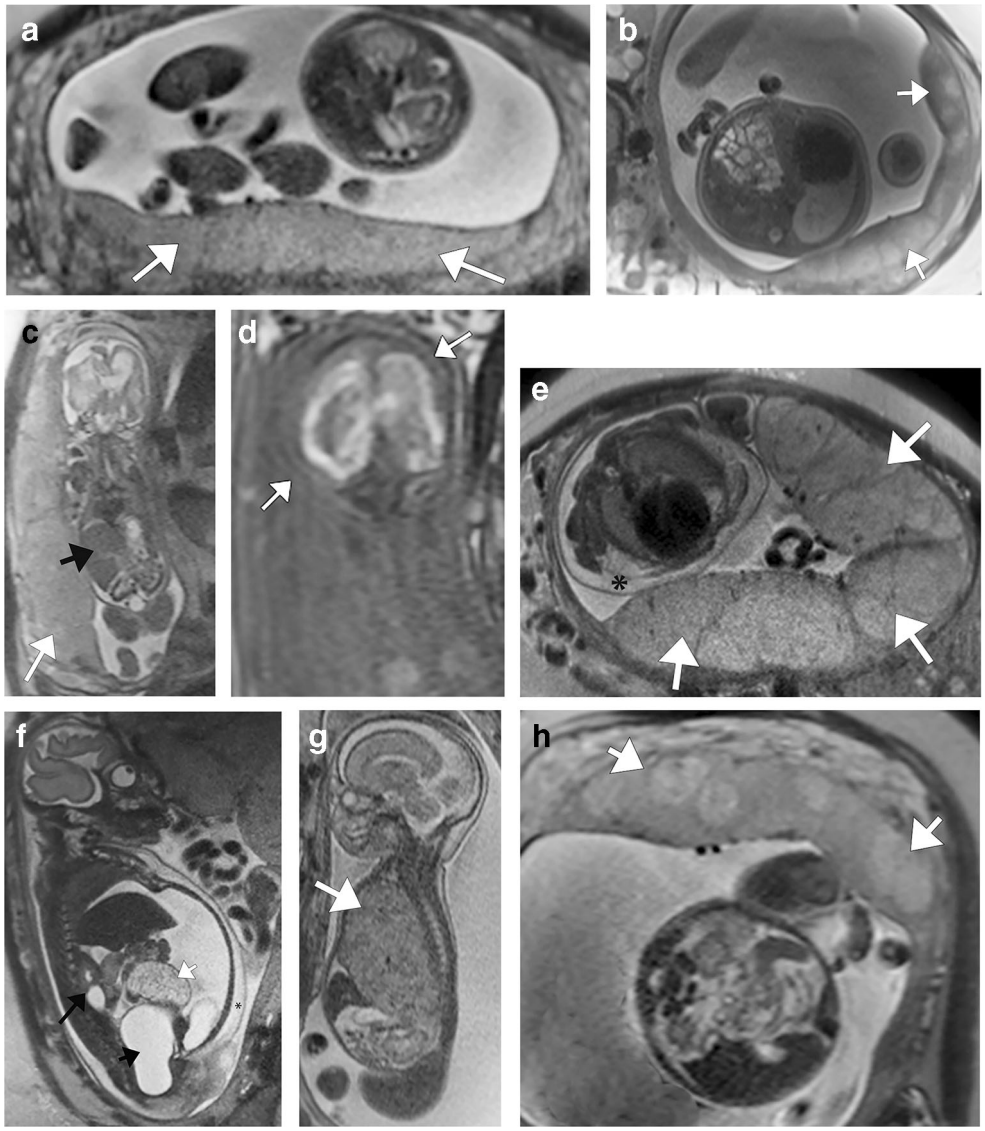

Fig. 7 Normal and abnormal appearance of the placenta. **a, b** Single-shot turbo spin-echo (SSTSE) MR images of the maternal pelvis show the normal appearance of the placenta in 22-week (**a**) and 34-week (**b**) fetuses. Note the homogeneity of the placenta in the second trimester, becoming more heterogeneous and with more distinct cotyledons or placentofetal units during the third trimester**. c, d** Coronal SSTSE images in a 21-week fetus show abnormally thickened placenta (*white arrow* in **c**; compare with **a**). The fetus also presented with hepatomegaly (*black arrow* in **c**), ascites and marked hemorrhagic and destructive changes in the brain, best seen in the coronal T1-weighted image (**d**). The constellation of findings was thought to be from an infectious etiology. **e, f** Axial (**e**) and sagittal (**f**) SSTSE MR images in a 29-week fetus with findings of cloaca and placentomegaly. The abnormally thickened and hyperintense placenta is denoted (*arrows* in **e**). Image (**f**) demonstrates abnormal kidney with pelvicaliectasis (*long black arrow*); a fluid-filled vagina (*short black arrow*) posterior to the bladder; colon containing enteroliths (*white arrow*), consistent with admixing of urine and a urorectal fistula; as well as soft-tissue thickening (*asterisk*). Also present were ascites, pulmonary hypoplasia and oligohydramnios. **g, h** Sagittal (**g**) and axial (**h**) SSTSE images in a 24-week fetus show a large T2-hypointense congenital pulmonary airway malformation (CPAM; *arrow* in **g**) and abnormally thickened and mature placenta, as denoted by the presence of multiple cotyledons (*arrows* in **h**) at this early gestational age

evaluating the fetus is determining lie and presentation. This allows for subsequent establishment of situs.

Position

As discussed, the localizer sequences are obtained in the three orthogonal planes with respect to the mother. These sequences are used to determine whether the fetus has a longitudinal, transverse or oblique lie. A longitudinal lie is when the long axis of the fetus is aligned with the long axis of the mother, either head up or head down. The lie is transverse when the long axis of the fetus is perpendicular to the mother's. Oblique is in between. Fetal presentation refers to the portion of the fetus in closest proximity to the birth canal. The presenting

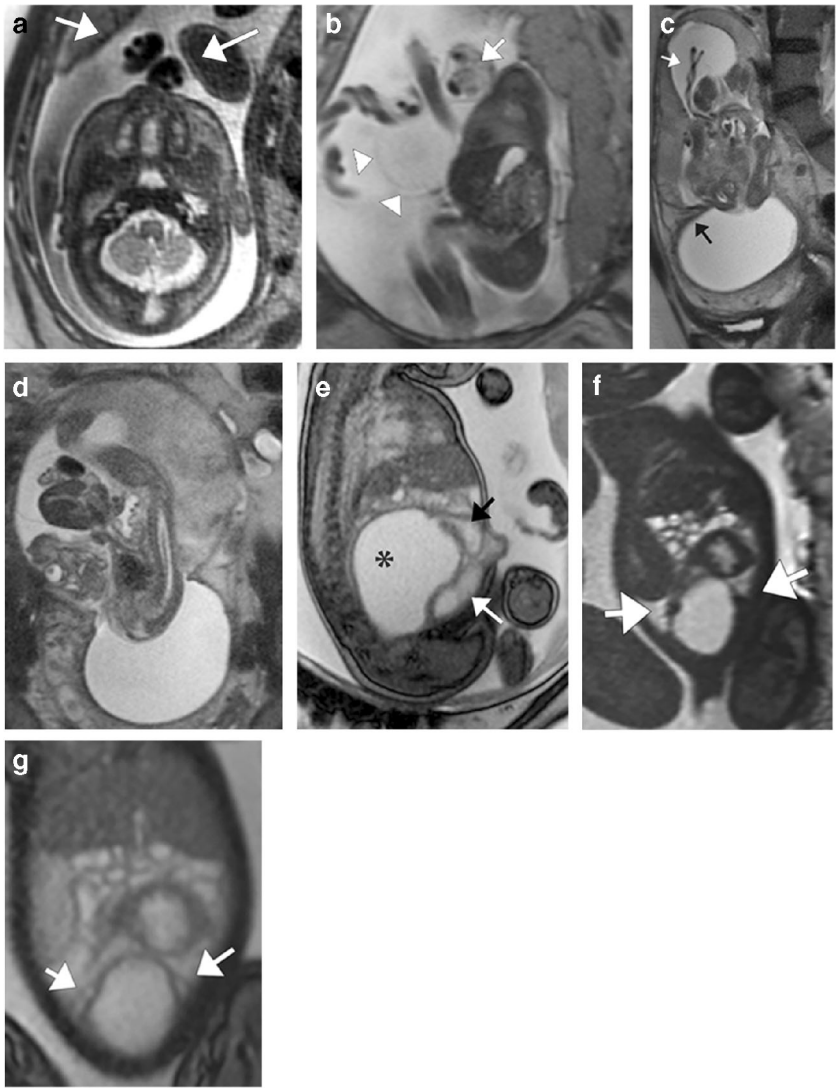

Fig. 8 The umbilical cord. **a** The three-vessel cord comprises two umbilical arteries and a vein, in a configuration that at MRI resembles a smiling face, as seen in this single-shot turbo spin-echo (SSTSE) cross-sectional image through the cord in a third-trimester gestation (*arrows*). **b** Cord masses are unusual; the sagittal SSTSE image in this 22-week fetus demonstrates the relatively common cord cyst (*arrowheads*) and the unusual cord hemangioma (*arrow*). **c, d** Sagittal (**c**) and coronal (**d**) SSTSE images through the pelvis in a woman carrying an 18-week fetus with limb–body wall defect. The fetus affected with this pathology might have short or unwound/underwound umbilical cord, as in this case (two vessels, underwound cord; *white arrow* in **c**). The placenta implanted in a thick uterine synechia (*black arrow* in **c**; note the maternal bladder at the lower edge of the image). The fetus, which had a giant skin-covered omphalocele, congenital heart disease and severe scoliosis, partially herniated through the synechia, as seen in (**d**). **e–g** The umbilical cord can be helpful in identifying the true bladder when this is in question, as in the cloacal case shown in this third-trimester gestation, where there are several cystic masses in the pelvis (**e**). Following the umbilical arteries retrograde from the cord should allow you to find the bladder, which should be hugged by the umbilical arteries (*arrows* in these coronal echoplanar and steady-state free precession [SSFP] sequences, **f** and **g**, respectively). This correlated to the anterior cystic structure in (**e**) (*white arrow*), whereas the posterior cystic structure in the sagittal SSFP image represents the uterus (*black arrow* in **e**), distended by the presence of hydrometrocolpos (*asterisk* in **e**)

part could be the fetal head or pelvis, resulting in cephalic or breech presentations, respectively. When the lie is transverse, the shoulder is often the presenting part.

Situs

It is essential to establish which side of the fetus is right, and which is left. Depending on the fetal position, the fetus's left or right side may be closest to the mother's spine. For example, in a fetus in breech position facing the maternal right, the fetus's right side is closer to the maternal spine and the left side is closer to the maternal abdominal wall. Contrarily, in a fetus in breech position facing the maternal left, the fetus's left side is closer to the maternal spine and the right side is closer to the maternal abdominal wall. One helpful strategy when resolving situs is to adopt the perspective of the fetus, and then

"consider your position" with respect to the mother. Other methods are available in the literature, such as the popular right-hand rule [41]. Having established fetal situs with respect to the mother, one can then determine whether the fetal organs are anatomically arranged. Specifically, that the heart, stomach and spleen are to the left, and the liver is to the right.

Fetal head, neck and spine

Brain

Imaging of the fetal brain is performed in three orthogonal planes (sagittal, coronal and axial) utilizing T2-weighted sequences. The sagittal plane should be acquired with the center slice including all the major midline structures on the same image, specifically the corpus callosum, the cerebral aqueduct, the pituitary infundibulum, and the cerebellar vermis. The coronal and axial planes are acquired parallel and perpendicular to the axis of the brainstem, respectively [42]. The field of view should include the tip of the nose to the occiput, the vertex to the craniocervical junction, and ear to ear.

Biometry is an essential component to determining the health of the fetal brain [42, 43]. One advantage of MRI over US is MR's utility for acquiring brain measurements regardless of fetal head positioning [44]. Measurements include, but are not limited to, the cranium, whole brain, corpus callosum, ventricular system, brainstem and cerebellum. They should be included in all reports.

Cortical sulcation occurs in a predictable pattern and allows for dating of pregnancy on fetal MRI (Fig. 9). Primary sulci develop first as a shallow depression and eventually deepen. With maturation, primary sulci develop branches that become secondary sulci. The secondary sulci will also branch, creating tertiary sulci. Table 2 summarizes the appearance of the main sulci according to the gestational age in which they are detectable in at least 75% of cases [44–46].

The brain parenchymal signal evolves with gestational age as well (Fig. 10). This reflects changes that happen during proliferation, cell migration, neuronal organization and maturation [47, 48]. At fewer than 20 weeks of gestation, fetal MRI shows three layers: the germinal matrix (T1 hyperintense/T2 hypointense), the intermediate layer (T1 hypointense/T2 hyperintense), and the cortex (T1 hyperintense/T2 hypointense). Between 20 weeks and 28 weeks, a five-layer appearance is evident: the germinal matrix, which includes both the ventricular zone and ganglionic eminences (T1 hyperintense/T2 hypointense) of the subventricular zone; the periventricular fiber-rich zone (T1 hypointense/T2 hyperintense), also known as the cell-sparse layer of the subventricular zone (most medial lateral compartment); the intermediate zone (T1 hyperintense/T2 hypointense), which represents the fetal white matter and contains the cell-dense areas of subventricular zone; the subplate (T1 hypointense/T2 hyperintense); and the cortical plate (T1 hyperintense/T2 hypointense), which thickens with increasing gestational age because of increased cell number and organization.

Myelination is a process that begins in the fetus and continues for years during the postnatal period. T1-hyperintense signal from the lipid content of myelin is seen in the tegmentum of the pons from 23 weeks of gestation, and in the posterior limb of the internal capsule from 31 weeks of gestation, both with corresponding T2-hypointense signal [49].

The ventricles develop from cavities of the primitive cerebral vesicles. The lateral ventricles are visible at 13–14 weeks of gestation and change in size and shape with cerebral development. Before 16 weeks of gestation, the primitive lateral ventricles appear large and globular. With increasing gestational age, the ventricles narrow and become adult-like in configuration. The atrial width is not dependent on gestational age and remains constant throughout the second and third trimesters, with ventriculomegaly being greater than 10 mm. The third ventricle should not exceed 4 mm and the fourth ventricle should not exceed 7 mm. Fetal ventriculomegaly is the most common central nervous system (CNS) anomaly detected by prenatal ultrasound. The causes of ventriculomegaly are variable and can be broadly divided mechanistically into obstructive and nonobstructive etiologies. This is described in detail in a separate article that is part of this symposium.

Face and neck

Like the brain, the face and neck should be evaluated in three orthogonal planes. The sagittal midline plane is important for defining the facial profile, including the nose, chin and soft palate (Fig. 11). Symmetry of the face, the lips, nose and orbits can be assessed in either the coronal or axial planes. The primary palate is derived from the intermaxillary segment and includes the alveolar ridge. The secondary palate is composed of the remainder of the hard and soft palate [50]. The palate is visualized in more than 80% of fetuses at up to 27 weeks of gestation. The sagittal plane is helpful in evaluating the secondary palate, including the soft palate. In our experience, the coronal slices are a helpful adjunct in assessing the palate and for depicting clefts. The tooth buds form a continuous arc and are best visualized on axial views of the maxilla and mandible.

The globes have a physiological nonelliptical shape up to 22–29 weeks of gestation, with convexity of the posterolateral margins. After 29 weeks of gestation, they develop an elliptical or near-round shape [50]. Any asymmetry of the globes should be considered pathological. Hyaloid vasculature can be seen in most fetuses up to 19 weeks of gestation but is not visible after 24 weeks. The lenses appear as hypointense structures on T2-weighted imaging and should be evaluated. Growth charts for the fetal lens and orbit, as well as the measurements of binocular and interocular distances, have been determined [51].

The pharynx and larynx are filled with amniotic fluid and are therefore easily detected on T2-weighted images. The laryngeal

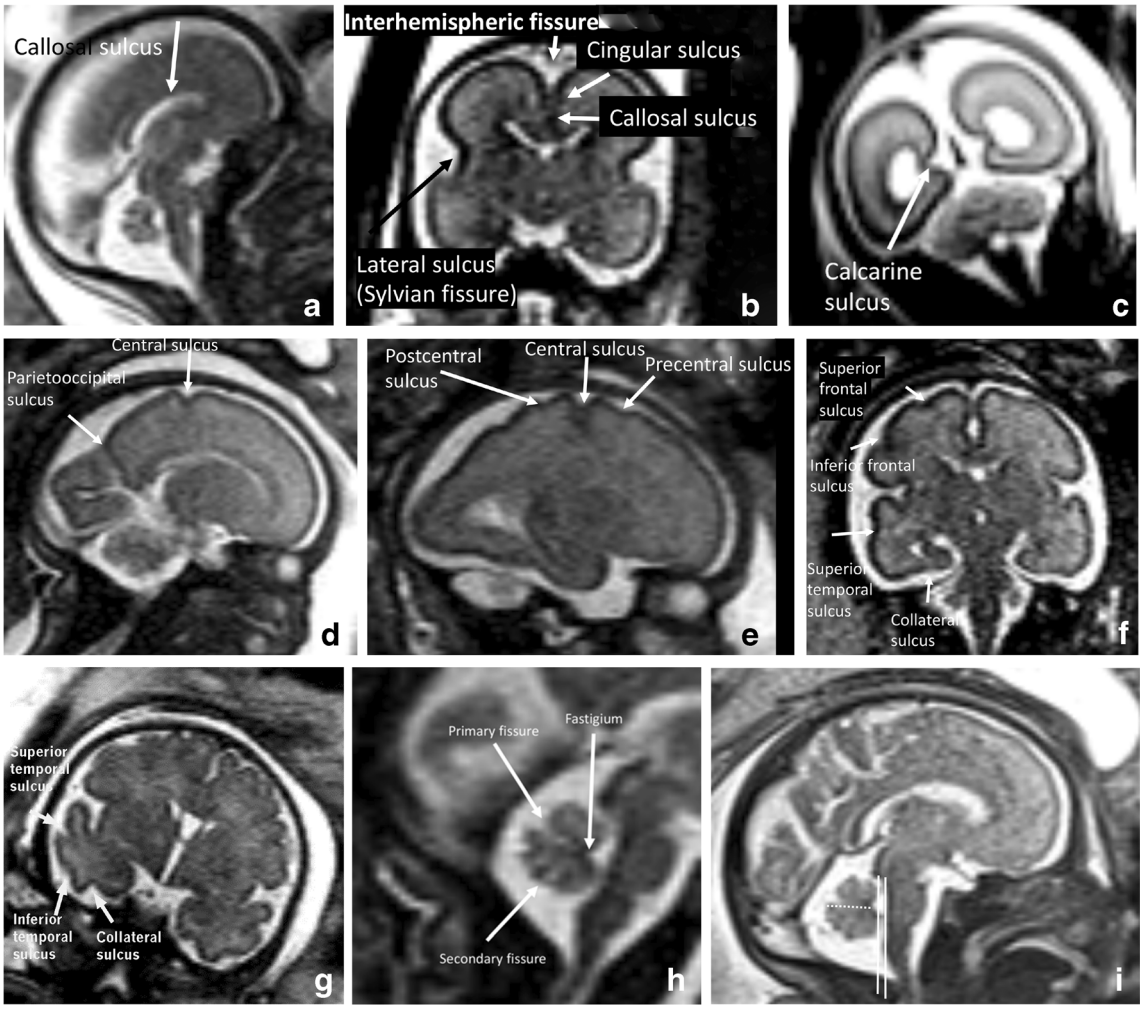

Fig. 9 Evolution of cortical sulcation in the fetal brain seen in coronal and sagittal single-shot turbo spin-echo (SSTSE) MR images. **a–g** Normal progressive development of cortical sulcation demonstrated in fetuses at different gestational ages. Sagittal (**a**) and coronal (**b** and **c**) images demonstrate the normal brain sulcation of a 23-week fetus, sagittal (**d** and **e**) and coronal (**f**) images show the normal brain anatomy at 27-weeks, and coronal image (**g**) shows normal sulcation at 37 weeks. **h, i** Coronal images demonstrate normal development of cerebellum at 27 weeks (**h**) and 34 weeks (**i**), showing the main vermian fissures. The fastigium–declive line is the dashed line. The tegmentum-vermian angle is drawn by a line parallel to the tegmentum of the pons and another line drawn along the anterior surface of the vermis. In this case, the tegmentum–vermian angle is close to 0°

folds and epiglottis can gradually be identified with advancing gestational age. The cervical esophagus is visible as a tubular fluid-filled structure during swallowing movements.

The fetal thyroid is best identified on T1-weighted imaging, where it appears conspicuously hyperintense relative to the surrounding tissues (Fig. 12). It should be identified in normal fetuses after 18 weeks of gestation.

The cervical great vessels can be seen using axial or coronal SSFP (Fig. 12), or on all planes with T2-weighted SSFSE images [52].

Spine

Similar to the brain and face/neck, T2-weighted images are the most useful in assessing the spine and surrounding soft tissues. The entire extent of the spine should be covered in three orthogonal planes. The axial plane is useful for determining the level of termination of the conus medullaris in cases of suspected cord tethering as well as the location of the neural placode in fetuses with neural tube defects. It should be noted that the level of termination of the conus medullaris is variable in the fetal and neonatal period, and adult parameters might not be applicable at these ages. Coronal and sagittal images can help in identifying abnormal curvatures caused by segmentation anomalies as well as provide an overview of the gastrointestinal and urological systems, which might be affected in syndromes that involve the spine. EPI sequences can help in assessing the bony components of the fetal spine. Table 3 provides a checklist for examining the fetal central nervous system with MRI.

Table 2 Appearance of main sulci by gestational age (GA) in weeks

Sulci	GA (weeks) at visualization (>75% of fetuses)	Best imaging plane
Interhemispheric fissure	14–15	Axial, coronal
Lateral (Sylvian fissure)	16	Axial, coronal, sagittal
Callosal	22–23	Coronal
Parieto-occipital	22–23	Sagittal
Calcarine	24–25	Coronal
Cingular	24–25	Coronal
Collateral	24–26	Coronal
Central	26	Axial, sagittal
Precentral	27	Axial, sagittal
Postcentral	28	Axial, sagittal
Superior temporal	27	Coronal
Superior frontal	29	Coronal
Inferior frontal	29	Coronal
Inferior temporal	32	Coronal
Secondary insular	34	Axial

Body

Thorax

The non-aerated fetal lungs contain a significant amount of fluid. As a result, the trachea, bronchi and lungs are T2 hyperintense relative to the chest wall muscles. With advancing gestation, the fetal lungs should increase in both volume and T2 hyperintensity [9]. Increasing production of alveolar fluid accounts for the MR-apparent signal increase on fluid-sensitive sequences. The normal fetal lungs exhibit homogeneous signal intensity. Low signal intensity of the fetal lungs at later gestational ages is indicative of pulmonary hypoplasia [53] (Fig. 13). Heterogeneous T2-hyperintense tubular branching structures might be seen in the context of "nutmeg lung," a pattern associated with lymphangiectasia [54, 55].

Accurate prenatal diagnosis and quantification of pulmonary hypoplasia are profoundly important because its severity is strongly linked to postnatal outcome [56]. One potential advantage of MRI over US is MR's slightly higher prognostic accuracy in estimating fetal lung volumes [57]. To acquire

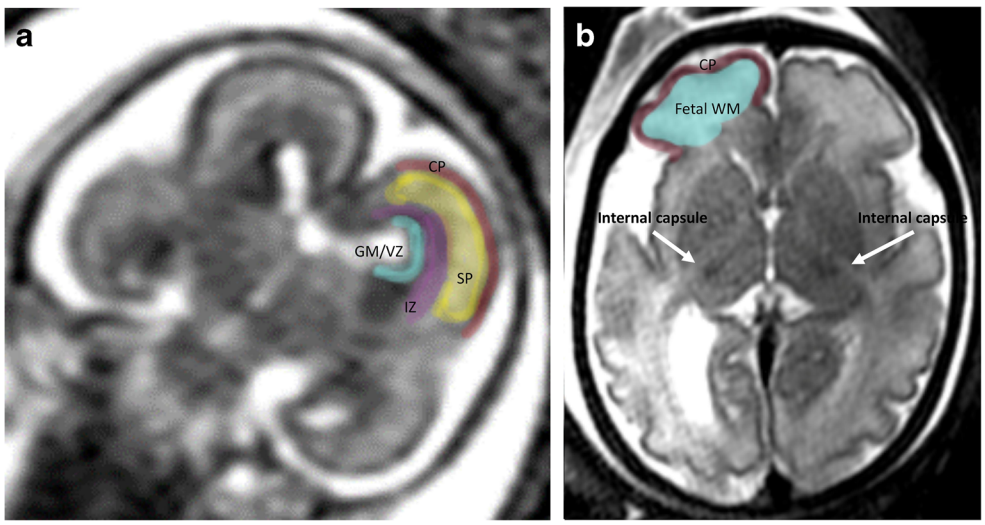

Fig. 10 Multilayered development of the cerebral parenchyma. **a, b** Coronal single-shot turbo spin-echo (SSTSE; **a**) MR image shows a 23-week fetus, and axial SSTSE (**b**) shows a 35-week fetus. Multilayered pattern of the fetal brain is depicted up to 28 weeks of gestation, as seen in (**a**). From 28 weeks of gestation onward, there is gradual blurring of the layers, with disappearance of the subplate and germinal matrix yielding to a two-layer pattern at later gestational ages (**b**). At 34 weeks, the deep gray nuclei are hypointense on T2- and hyperintense on T1-weighted images, contributing to the visualization of the posterior limb of the internal capsule (*arrows*). *CP* cortical plate (*red* in **a** and **b**), *GM/VZ* germinal matrix/ventricular zone (*light blue* in **a**), *IZ* intermediate zone (*purple* in **a**), *SP* subplate (*yellow* in **a**), *WM* white matter (*blue* in **b**)

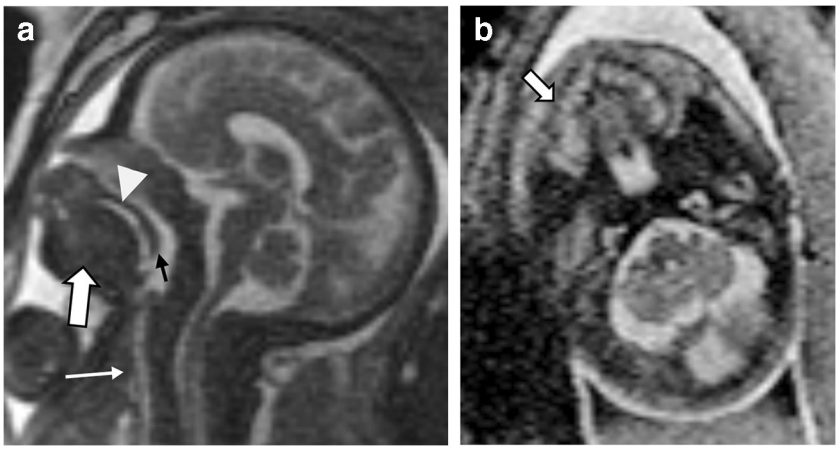

Fig. 11 Fetal mouth and swallowing. **a** Sagittal 2-D steady-state free precession MR image shows the hard palate (*arrowhead*) and the most posterior part of the soft palate (*black arrow*) in a 33-week fetus. Note fetal tongue (*thick white arrow*) and trachea (*thin white arrow*). **b** Axial single-shot turbo spin-echo MR image at the level of the maxilla in a 28-week fetus shows T2-hypointense tooth buds (*arrow*)

these volumes, an ROI is separately placed over the cross-sectional area of each lung, on every transverse image (slice) through the lungs. The volume of each slice is then calculated by multiplying the cross-sectional area by the combined slice thickness. To increase the accuracy of the measured volume, there should be no interslice gap. The volume of the entire right and left lungs is then determined by summing the volumes of each slice [56]. These observed lung volumes can be compared to expected age-matched normative values [58, 59].

Intrathoracic and intra-abdominal structures can be distinguished by evaluating sagittal and coronal images at the level of the diaphragm. An inability to delineate the diaphragm should raise concern for congenital diaphragmatic hernia (CDH). The most common location for a CDH is at the posterior aspect of the left hemidiaphragm. When this is present, the radiologist should evaluate for the presence of any liver in the chest because that finding significantly worsens prognosis [60]. The EPI and T1-weighted sequences can be extremely helpful in differentiating the hypointense (EPI)/hyperintense (T1) liver from surrounding structures. MRI can also be used to distinguish intrathoracic meconium-filled loops of herniated bowel from congenital chest masses [9]. In addition to

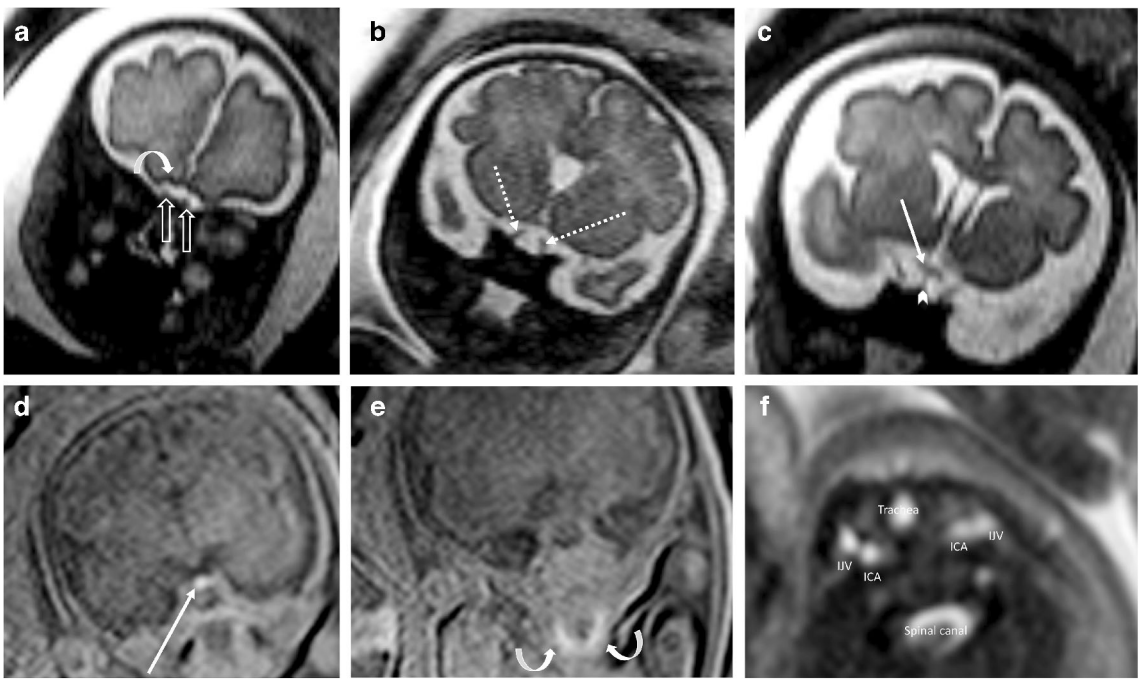

Fig. 12 Normal central nervous system (CNS) findings at fetal MR imaging. **a–c** Coronal single-shot turbo spin-echo images in a 30-week fetus. The olfactory bulbs (*straight arrows* in **a**) and olfactory sulcus (*curved arrow* in **a**) are better visualized when the pericerebral fluid spaces are large. Note the optic nerve (*dashed arrows* in **b**), optic chiasma (*arrow* in **c**) and pituitary stalk (*arrowhead* in **c**). **d, e** Coronal gradient echo T1-weighted MR images show the hypersignal intensity of the pituitary gland (*arrow* in **d**) and of the thyroid gland (*arrows* in **e**). **f** Axial steady-state free precession MR image at the level of the neck in this bright-blood sequence shows the great vessels of the neck. *ICA* internal carotid artery, *IJV* internal jugular vein

Table 3 Fetal central nervous system checklist

Main categories	Subcategories
✓ Biometry	
✓ Cerebral sulcation/gyration	
✓ Cerebral signal intensity and layers	
✓ Location of the tentorium and size of the posterior fossa	
✓ Cerebellar vermis	○ Primary fissure and fastigial point
	○ Ratio "above:below" the fastigium–declive line
	○ Tegmentum–vermian angle (closure of the 4th ventricle)
	○ Vermian lobulation
✓ Craniocervical junction and foramen magnum	
✓ Morphology of the pons	
✓ Other structures	○ Pituitary gland and stalk
	○ Optic chiasma
	○ Olfactory bulbs and sulci
✓ Ventricular system and pericerebral spaces	○ Cavum septum pellucidum
	○ Corpus callosum
✓ Facial profile and its proportions	
✓ Facial symmetry	
✓ Eye globes and lenses	
✓ Ears	
✓ Palate, lips and tooth buds	
✓ Pharynx and larynx	
✓ Thyroid gland	
✓ Great vessels of the neck	
✓ Spine — curvature, spinal cord with its termination, soft tissues, bony components	

congenital diaphragmatic hernia, the commonest thoracic abnormalities studied by MR imaging include congenital pulmonary airway malformation (CPAM), bronchopulmonary sequestration and congenital bronchogenic cyst [61, 62].

The fetal thymus, visualized predominantly in the third trimester, should not be confused with a mass. Located within the anterior mediastinum, it has a gently lobulated contour and is iso- to slightly hypointense compared to the lungs on all sequences. Thymic hypo/aplasia should raise concern for DiGeorge (or other 22q11 deletion type) syndrome [63].

Fetal echocardiography remains the gold standard for evaluating the fetal heart. Visualizing the heart chambers by MR is challenging because of its small size and high pulsation rate. The appearance of the heart and vessels is dependent on the sequence. Bright-blood SSFP sequences are best for visualizing the heart and vessels because the hyperintense blood provides excellent contrast against the myocardium. With T2-weighted SSFSE sequences, the heart and vessels appear hypointense, mainly because of flow void artifact resulting from blood flow. Fetal MRI can detect positional anomalies, reveal cardiomegaly or discrepant chamber sizes, and demonstrate cardiac tumors. With recent technical advances and improved image quality, the clinical utility of fetal cardiovascular MRI is likely to improve [64].

Gastrointestinal tract

Fluid-containing abdominopelvic organs such as the esophagus, stomach, bowel, urinary collecting systems and bladder are T2 hyperintense. The esophagus is usually decompressed and might not be seen. It might be easily visualized when the fetus is swallowing, or if distended in cases of reflux or distal obstructions. The stomach can be easily recognized as a saccular fluid-filled structure, and its expected location in the left upper quadrant should be confirmed. A small stomach should prompt a search for a cause of impaired swallowing, for example from mechanical obstruction from a neck mass, or in cases of tracheoesophageal fistula. A persistently large stomach should raise concern for more distal bowel obstruction.

Early in gestation, the proximal and distal small intestine show similar signal characteristics. As fetal development progresses, swallowing and gastric emptying increase. The ingested amniotic fluid renders the proximal intestine hyperintense on T2- and hypointense on T1-weighted sequences. Swallowing occurs by 12 weeks of gestation and can be evaluated on cine imaging. Fluid resorption in the distal small bowel results in relative T2 hypointensity distally, compared to the more proximal small bowel.

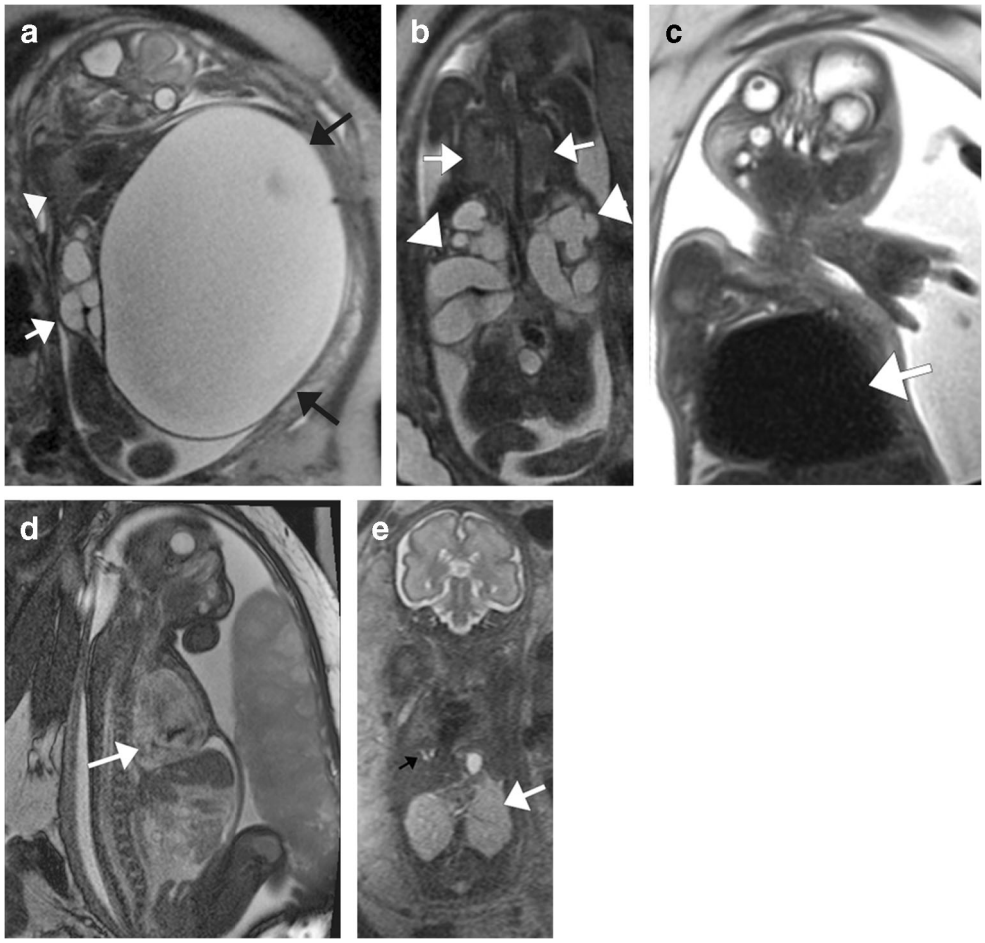

Fig. 13 Examples of pulmonary hypoplasia. **a, b** Sagittal (**a**) and coronal (**b**) single-shot turbo spin-echo (SSTSE) MR images in a 22-week fetus with markedly enlarged bladder (*black arrows* in **a**) shows findings of pelvicaliectasis and marked ureterectasis (*white arrow* in **a**, *arrowheads* in **b**), marked pulmonary hypoplasia (*arrowhead* in **a**, *arrows* in **b**) and oligohydramnios. Together with a small colon (not shown) in this female fetus, the findings were consistent with megacystis microcolon intestinal hypoperistalsis syndrome. **c, d** Coronal black-blood SSTSE (**c**) and sagittal steady-state free precession (SSFP) white-blood (**d**) sequences of the thorax in a 33-week fetus with Ebstein anomaly (*arrows*). Note that the entire thoracic cavity is essentially occupied by the markedly enlarged heart, with the lungs only accounting for 19% of the expected value in this case, and barely seen. Placentomegaly and a small amount of ascites were also present at the time of imaging. **e** Coronal SSTSE MR image demonstrates autosomal-recessive polycystic kidney disease in a 29-week fetus with Caroli disease. Note the relatively small lungs (50% of the expected lung volume), the enlarged and T2-hyperintense bilateral kidneys (*white arrow*), and anhydramnios. Some biliary radicals were dilated in this fetus (*black arrow*), who developed postnatal hepatic fibrosis

The MR appearance of the colon depends on the presence of meconium. Meconium is composed of intestinal secretions, desquamated epithelium and swallowed amniotic fluid [65]. The high protein content makes it appear hyperintense on T1-weighted images. At 13 weeks of gestation, it is first produced in the small bowel, and then slowly migrates down through the colon. At 20 weeks of gestation, functional obstruction of the anal canal results in accumulation of meconium in the large bowel. With increasing gestational age, the meconium column progressively fills proximally, eventually reaching the small bowel.

The caliber of the bowel increases with advancing gestational age. At 20 weeks of gestation, the small bowel measures 2–3 mm in diameter, with diameters reaching up to 7–8 mm beyond 35 weeks of gestation [65]. The caliber of the colon is 3–4 mm at 20 weeks of gestation and reaches up to 15 mm by 35 weeks. When radiologists recognize the diameter and signal changes of the small and large bowel, they can use MRI to both diagnose and locate the level of bowel obstruction in cases of atresia [66] (Fig. 14).

Liver

The liver is responsible for the majority of early fetal erythropoiesis and therefore contains a high amount of iron-laden hemoglobin [67]. This contributes to its characteristic high T1, low T2 and low EPI signal. Fetal MR imaging can be of particular value for assessing cystic lesions, for example differentiating a choledochal anomaly from an intrahepatic cyst. The gallbladder is identified as a cystic structure beneath the

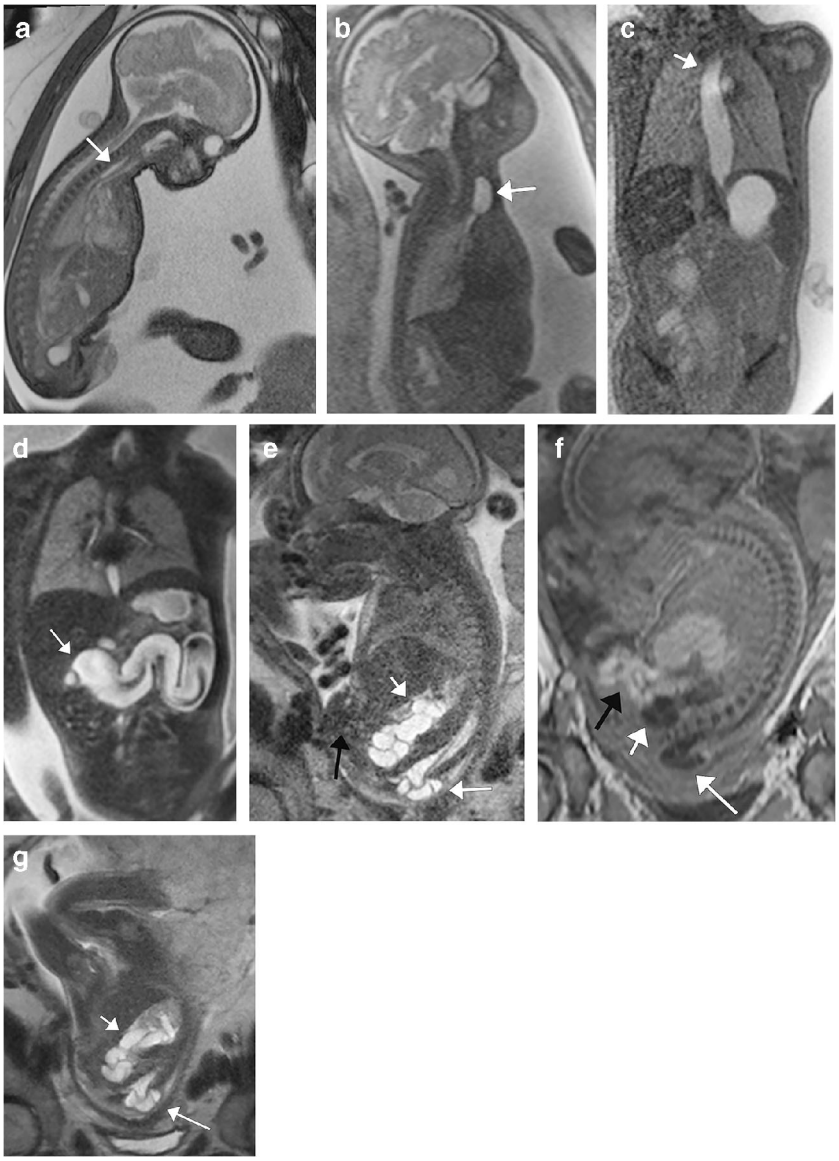

Fig. 14 Anomalies of the alimentary tract. **a** Sagittal steady-state free precession (SSFP) MR image in a 32-week fetus with tracheoesophageal fistula shows an intermittent esophageal pouch (*arrow*). Also present were a small stomach and polyhydramnios (not shown). **b** This 33-week fetus with a large pouch (*arrow*) had esophageal atresia without fistula, as seen on sagittal single-shot turbo spin-echo (SSTSE) MR image. **c** Coronal SSTSE image demonstrates marked esophageal distension (*arrow*) in a 35-week fetus with prenatal diagnosis of duodenal atresia and added postnatal diagnosis of alveolar capillary dysplasia. **d** Coronal SSTSE image shows dilated, undulating bowel (*arrow*) in a 27-week fetus with postnatal diagnosis of jejunal atresia. **e–g** Abnormal bowel distribution in a 29-week fetus with cloacal exstrophy on sagittal SSTSE image (**e**), sagittal T1-W (**f**) and coronal SSTSE with respect to maternal axis (**g**) MR images. Non-visualization of the bladder in a background of normal amniotic fluid should raise the suspicion of exstrophy. Sagittal images depict abnormal meconium distribution (*black arrows*). The absence of a rectal meconium column anterior to the sacral spine as well as the presence of a closed spinal defect (*long white arrows*) should further suggest cloacal exstrophy. Coronal SSTSE image with respect to the maternal axis (**g**) demonstrates that the right kidney is duplicated and malrotated. Diffuse uteterectasis of the duplicated moieties is noted (*short white arrows*)

liver edge and is apparent by 18 weeks of gestation. The biliary tree is not appreciated under normal circumstances. The spleen becomes detectable at about 20 weeks of gestation, located dorsal and lateral to the stomach. The signal intensity is homogeneous and similar to that of the liver, but demonstrates progressive signal loss throughout gestation. This is thought to be secondary to alterations in the ratio of white-to-red pulp. Anomalies of splenic position and number might be present in heterotaxy syndromes. The topographical relations and signal intensities of the fetal pancreas are similar to those in adults, although they are usually difficult to see at lower field strengths [16].

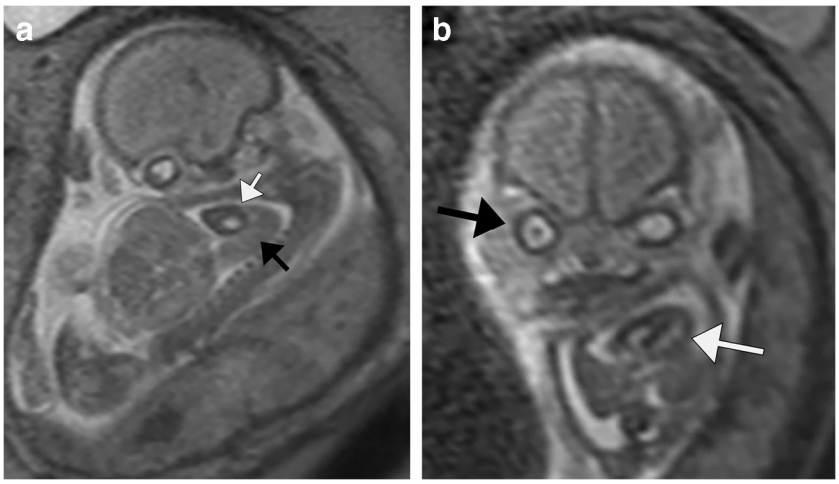

Fig. 15 Unexpected fetal demise. **a, b** Sagittal and coronal single-shot turbo spin-echo MR images in a 22-week fetus imaged to evaluate abnormal bowel. The images show findings of fetal demise, including bright signal in the cardiac chambers in this black-blood sequence (*white arrows*), indistinctness of the soft tissues throughout, with loss of gray/white matter differentiation. The lungs are small (*black arrow* in **a**). Note also the dark orbital rim (*black arrow* in **b**), another MR marker of fetal demise

Adrenal glands, kidneys and bladder

The adrenal glands are relatively large in the fetus, and they markedly increase in size during the second and third trimesters. They are already detectable at 20 weeks of gestation and are well demarcated by the surrounding perinephric adipose tissue. They are best appreciated on T2-weighted sequences, in which they appear peripherally hypo- and centrally hyperintense. This central hyperintensity diminishes after 35 weeks of gestation, rendering the glands less conspicuous.

Throughout gestation, the fetal kidneys change significantly in length in T2-weighted signal intensity and apparent diffusion coefficient (ADC) values [68]. On T2-weighted images, the renal cortex is hypointense to the medulla, with the signal difference becoming increasingly conspicuous throughout gestation. ADC values tend to decrease throughout gestation. The most common cause of prenatally detected urinary tract dilatation is ureteropelvic junction obstruction [69]. The dilated upper collecting system might hang down, and this should not be confused with hydroureter. Detection of a genitourinary abnormality should prompt a search for possible sequelae of the Potter sequence, including lung hypoplasia and oligohydramnios.

The urinary bladder appears as a fluid-filled structure in the pelvis. Dilatation of the renal collecting systems and an abnormally distended urinary bladder suggest lower urinary tract obstruction (e.g., from posterior urethral valves). In males, the scrotum and penis are often recognized, and advances in imaging quality have improved detection of the normal female genitalia. Fetal MRI can also be helpful in identifying ovarian cysts in the female abdomen or pelvis.

Anterior abdominal wall

The anterior abdominal wall should be evaluated for the site of cord insertion and for any defects, as can be seen with gastroschisis, omphalocele or exstrophies.

Musculoskeletal development

Ultrasound remains an optimal modality for assessing the fetal skeleton, including measuring long bones and detecting subtle findings that might involve the distal appendages. With improvements in MR imaging, techniques such as EPI and thick-slab T2-weighted sequences (which cover the whole fetus) can be helpful in evaluating fetal bone and skeletal development [70]. The normal cartilaginous epiphysis might be seen as hyperintense on EPI. Apart from a few exceptions such as the diaphragm, the homogeneous T2-weighted hypointensity of individual muscles prevents their delineation. MRI can show abnormal thickness and contour, which might indicate the presence of a neuromuscular disorder. Wide-field-of-view sequences can demonstrate fixed or abnormal positioning of the fetus within the uterus. Abnormal thickening and edema of the subcutaneous soft tissues might indicate focal pathology (such as amniotic band syndrome) or a diffuse abnormality such as fetal hydrops. In instances of suspected skeletal abnormality, US has only 40–60% sensitivity in making the correct diagnosis. In these cases, ultra-low-dose CT can be of great value [71, 72].

The fetal musculoskeletal system is evaluated in-depth in the article "Magnetic resonance imaging of the fetal musculoskeletal system" by Chauvin et al., found in this issue of *Pediatric Radiology*.

Recognizing magnetic resonance findings of fetal demise

Sometimes a fetal MR is the first imaging modality performed when fetal demise occurs. Recognizing a fetal demise is crucial to avoiding continued scanning and to institute appropriate treatment and counseling.

When the death has occurred weeks prior to scanning, the findings are obvious (progressively small fetus, blurring of all

Table 4 Sample report template for a fetal MR imaging study, adapted from Beth M. Kline-Fath, Cincinnati Children's Hospital Medical Center

CLINICAL HISTORY: [..]

COMPARISON: [..]

PROCEDURE COMMENTS: MRI was performed without contrast to evaluate the uterus and fetus.

FINDINGS

The assigned gestational age of the pregnancy is [..] weeks, [..] days.

Maternal findings: None.

Findings of pregnancy

Pregnancy: Singleton.
Placental location:
Placenta previa: No.
Placental signal: Homogeneous.
Placental thickness: [..] cm.
Uterus: Normal.
Cervix: Closed.
Cervical length: [..] cm.

Fetal findings

Fetal position: Vertex.
Fetal motion: Normal.
Amniotic fluid volume: Normal.
Number of vessels in umbilical cord: Three.
Umbilical cord insertion site: Paracentral (series number, image number)

Brain

Calvarial shape: Normal.
Head size: Normal.
Frontal-occipital diameter: [..] mm.
Bone biparietal diameter: [..] mm.
Cerebral biparietal diameter: [..] mm.
Sulcation: Normal.
Ventricles: Normal.
Cavum sept um pellucidum: Normal.
Germinal matrix: Normal.
Cerebral venous sinuses: Normal.
Brain parenchyma signal: Normal.
Corpus callosum: Normal.
Brainstem morphology: Normal.
AP pons diameter: [..] mm.
Cerebellum: Normal.
Transverse cerebellar diameter: [..] mm.
Cerebellar vermis: Normal.
Foliation: Normal.
Vermis (CC x AP): [..] mm.
Craniocervical junction: Normal.
Extraaxial fluid spaces: Normal.

Face/neck

Oropharynx/cervical airway: Normal.
Facial profile: Normal.
Eyes: Normal.
Lips and nose: Normal.
Mandible: Normal.
Ears: Normal.
Nuchal fold: Normal.

Spine

Vertebrae: Normal.
Spinal canal: Normal.
Spinal cord: Normal.
Conus position: Normal.

Chest

Chest size/shape: Normal.
Airway: Normal.
Mediastinum/thymus: Normal.
Lungs: Normal.
Heart: Normal.
Aorta: Normal.

Abdomen

Abdominal wall/soft tissues: Normal.
Situs: Normal.
IVC/aorta: Normal.
Liver: Normal.
Gallbladder: Normal.
Spleen: Normal.
Stomach: Normal.
Small bowel: Normal.
Colon/rectum: Normal.
Right kidney: Normal.
Left kidney: Normal.
Urinary bladder: Normal.
Genitalia: Normal.

Extremities: Normal.

Note: Detailed evaluation of the extremities is limited on fetal MRI.

IMPRESSION: Normal MRI of the fetus.

AP anteroposterior, *CC* craniocaudal, *IVC* inferior vena cava

soft-tissue planes). When the death has occurred within hours or days, the most important finding is an absent signal void in the cardiac chambers as seen on SSTSE sequences [73]. Eventually there is blurring of soft-tissue planes, loss of differentiation of gray/white matter in the brain, development of pleural effusions, and non-visualization of stomach and bladder (Fig. 15). Cine images might help document lack of cardiac motion.

Reporting

Structured reporting is increasingly supported by many national and international radiology societies. Standardization of report structure ensures completeness and comparability of reports, while standardized language minimizes ambiguity. A structured report serves as a mental checklist and may educate trainees by providing a systematic approach to clinical interpretation. Table 4 provides a sample template that can be used to report the findings on a general fetal MRI.

Conclusion

MRI can play an important complementary role to US by providing excellent visualization of both the fetus and extrafetal structures, with superior tissue contrast. Interpreting and reporting these studies might be unfamiliar to many radiologists. Adopting a systematic approach, recognizing what is normal, and using a checklist and a structured reporting template might aid the radiologist in working through these cases. As imagers we can help provide information that is vital for prognostication, a crucial component of obstetric imaging and care.

Compliance with ethical standards

Conflicts of interest None

References

1. Graves CE, Harrison MR, Padilla BE (2017) Minimally invasive fetal surgery. Clin Perinatol 44:729–751
2. Pedreira DA (2016) Advances in fetal surgery. Einstein 14:110–112
3. de Laveaucoupet J, Audibert F, Guis F et al (2001) Fetal magnetic resonance imaging (MRI) of ischemic brain injury. Prenat Diagn 21:729–736
4. Bulas D, Egloff A (2013) Benefits and risks of MRI in pregnancy. Semin Perinatol 37:301–304
5. Valeviciene NR, Varyte G, Zakareviciene J et al (2019) Use of magnetic resonance imaging in evaluating fetal brain and abdomen malformations during pregnancy. Medicina 55:55
6. Levine D (2013) Timing of MRI in pregnancy, repeat exams, access, and physician qualifications. Semin Perinatol 37:340–344
7. Manganaro L, Antonelli A, Bernardo S et al (2018) Highlights on MRI of the fetal body. Radiol Med 123:271–285
8. Frates MC, Kumar AJ, Benson CB et al (2004) Fetal anomalies: comparison of MR imaging and US for diagnosis. Radiology 232:398–404
9. Saleem SN (2014) Fetal MRI: an approach to practice: a review. J Adv Res 5:507–523
10. Brugger PC, Stuhr F, Lindner C, Prayer D (2006) Methods of fetal MR: beyond T2-weighted imaging. Eur J Radiol 57:172–181
11. van Doorn M, Oude Rengerink K, Newsum EA et al (2016) Added value of fetal MRI in fetuses with suspected brain abnormalities on neurosonography: a systematic review and meta-analysis. J Matern Fetal Neonatal Med 29:2949–2961
12. Snyder E, Baschat A, Huisman T, Tekes A (2018) Value of fetal MRI in the era of fetal therapy for management of abnormalities involving the chest, abdomen, or pelvis. AJR Am J Roentgenol 210:998–1009
13. Aughwane R, Ingram E, Johnstone ED et al (2020) Placental MRI and its application to fetal intervention. Prenat Diagn 40:38–48
14. Yen CJ, Mehollin-Ray AR, Bernardo F et al (2019) Correlation between maternal meal and fetal motion during fetal MRI. Pediatr Radiol 49:46–50
15. Yamashita Y, Namimoto T, Abe Y et al (1997) MR imaging of the fetus by a HASTE sequence. AJR Am J Roentgenol 168:513–519
16. Victoria T, Johnson AM, Edgar JC et al (2016) Comparison between 1.5-T and 3-T MRI for fetal imaging: is there an advantage to imaging with a higher field strength? AJR Am J Roentgenol 206:195–201
17. Saleem SN (2008) Feasibility of MRI of the fetal heart with balanced steady-state free precession sequence along fetal body and cardiac planes. AJR Am J Roentgenol 191:1208–1215
18. Afacan O, Estroff JA, Yang E et al (2019) Fetal echoplanar imaging: promises and challenges. Top Magn Reson Imaging 28:245–254
19. Tanacan A, Orgul G, Aydin E et al (2019) Antenatal management and outcomes of pregnancies with congenital diaphragmatic hernia. J Neonatal Perinatal Med. https://doi.org/10.3233/NPM-190266
20. Amin RS, Nikolaidis P, Kawashima A et al (1999) Normal anatomy of the fetus at MR imaging. Radiographics 19:S201–S214
21. Mitter C, Jakab A, Brugger PC et al (2015) Validation of in utero tractography of human fetal commissural and internal capsule fibers with histological structure tensor analysis. Front Neuroanat 9:164
22. Limperopoulos C, Tworetzky W, McElhinney DB et al (2010) Brain volume and metabolism in fetuses with congenital heart disease: evaluation with quantitative magnetic resonance imaging and spectroscopy. Circulation 121:26–33
23. Roy CW, van Amerom JFP, Marini D et al (2019) Fetal cardiac MRI: a review of technical advancements. Top Magn Reson Imaging 28:235–244
24. Moore RJ, Strachan BK, Tyler DJ et al (2000) In utero perfusing fraction maps in normal and growth restricted pregnancy measured using IVIM echo-planar MRI. Placenta 21:726–732
25. Korostyshevskaya AM, Prihod'ko IY, Savelov AA, Yarnykh VL (2019) Direct comparison between apparent diffusion coefficient and macromolecular proton fraction as quantitative biomarkers of the human fetal brain maturation. J Magn Reson Imaging 50:52–61
26. Webb JA, Thomsen HS, Morcos SK, Members of Contrast Media Safety Committee of European Society of Urogenital Radiology (2005) The use of iodinated and gadolinium contrast media during pregnancy and lactation. Eur Radiol 15:1234–1240
27. Wang PI, Chong ST, Kielar AZ et al (2012) Imaging of pregnant and lactating patients: Part 1, evidence-based review and recommendations. AJR Am J Roentgenol 198:778–784
28. Epelman M, Merrow AC, Guimaraes CV et al (2015) Extrafetal findings on fetal magnetic resonance imaging: a pictorial essay. Semin Ultrasound CT MR 36:550–567
29. Fainaru O, Almog B, Gamzu R et al (2002) The management of symptomatic hydronephrosis in pregnancy. BJOG 109:1385–1387
30. Masselli G, Gualdi G (2013) MR imaging of the placenta: what a radiologist should know. Abdom Imaging 38:573–587
31. Blaicher W, Brugger PC, Mittermayer C et al (2006) Magnetic resonance imaging of the normal placenta. Eur J Radiol 57:256–260
32. Bonel HM, Stolz B, Diedrichsen L et al (2010) Diffusion-weighted MR imaging of the placenta in fetuses with placental insufficiency. Radiology 257:810–819
33. Brown BP, Meyers ML (2020) Placental magnetic resonance imaging Part II: placenta accreta spectrum. Pediatr Radiol 50:275–284
34. Aguirre-Pascual E, Epelman M, Johnson AM et al (2014) Prenatal MRI evaluation of limb-body wall complex. Pediatr Radiol 44:1412–1420
35. Abramowicz JS, Sheiner E (2007) In utero imaging of the placenta: importance for diseases of pregnancy. Placenta 28:S14–S22
36. Sepulveda W (2019) Antenatal course and perinatal outcome after ultrasound detection of triple nuchal cord: a case series. J Matern Fetal Neonatal Med. https://doi.org/10.1080/14767058.2019.1659773
37. Moshiri M, Zaidi SF, Robinson TJ et al (2014) Comprehensive imaging review of abnormalities of the umbilical cord. Radiographics 34:179–196

38. Sandlin AT, Chauhan SP, Magann EF (2013) Clinical relevance of sonographically estimated amniotic fluid volume: polyhydramnios. J Ultrasound Med 32:851–863
39. Ounpraseuth ST, Magann EF, Spencer HJ et al (2017) Normal amniotic fluid volume across gestation: comparison of statistical approaches in 1,190 normal amniotic fluid volumes. J Obstet Gynaecol Res 43:1122–1131
40. Didier RA, Khrichenko D, Barrera CA et al (2019) Novel computerized analytic technique for quantification of amniotic fluid volume in fetal MRI. AJR Am J Roentgenol 213:W149–W152
41. Bronshtein M, Gover A, Zimmer EZ (2002) Sonographic definition of the fetal situs. Obstet Gynecol 99:1129–1130
42. Garel C (2004) The role of MRI in the evaluation of the fetal brain with an emphasis on biometry, gyration and parenchyma. Pediatr Radiol 34:694–699
43. Kyriakopoulou V, Vatansever D, Davidson A et al (2017) Normative biometry of the fetal brain using magnetic resonance imaging. Brain Struct Funct 222:2295–2307
44. Garel C, Chantrel E, Elmaleh M et al (2003) Fetal MRI: normal gestational landmarks for cerebral biometry, gyration and myelination. Childs Nerv Syst 19:422–425
45. Levine D, Barnes PD (1999) Cortical maturation in normal and abnormal fetuses as assessed with prenatal MR imaging. Radiology 210:751–758
46. Ben Sira L, Garel C, Leitner Y, Gross-Tsur V (2008) [Prenatal imaging of the fetal brain — indications and developmental implications of fetal MRI]. Harefuah 147:65–70, 93
47. Brisse H, Fallet C, Sebag G et al (1997) Supratentorial parenchyma in the developing fetal brain: in vitro MR study with histologic comparison. AJNR Am J Neuroradiol 18:1491–1497
48. Kostovic I, Judas M, Rados M, Hrabac P (2002) Laminar organization of the human fetal cerebrum revealed by histochemical markers and magnetic resonance imaging. Cereb Cortex 12:536–544
49. Girard N, Raybaud C, Poncet M (1995) In vivo MR study of brain maturation in normal fetuses. AJNR Am J Neuroradiol 16:407–413
50. Nagarajan M, Sharbidre KG, Bhabad SH, Byrd SE (2018) MR imaging of the fetal face: comprehensive review. Radiographics 38:962–980
51. Robinson AJ, Blaser S, Toi A et al (2008) MRI of the fetal eyes: morphologic and biometric assessment for abnormal development with ultrasonographic and clinicopathologic correlation. Pediatr Radiol 38:971–981
52. Fujii S, Nagaishi J, Mukuda N et al (2017) Evaluation of fetal thyroid with 3D gradient echo T1-weighted MR imaging. Magn Reson Med Sci 16:203–208
53. Kuwashima S, Nishimura G, Iimura F et al (2001) Low-intensity fetal lungs on MRI may suggest the diagnosis of pulmonary hypoplasia. Pediatr Radiol 31:669–672
54. Saul D, Degenhardt K, Iyoob SD et al (2016) Hypoplastic left heart syndrome and the nutmeg lung pattern in utero: a cause and effect relationship or prognostic indicator? Pediatr Radiol 46:483–489
55. Victoria T, Andronikou S (2014) The fetal MR appearance of 'nutmeg lung': findings in 8 cases linked to pulmonary lymphangiectasia. Pediatr Radiol 44:1237–1242
56. Osada H, Kaku K, Masuda K et al (2004) Quantitative and qualitative evaluations of fetal lung with MR imaging. Radiology 231: 887–892
57. Kastenholz KE, Weis M, Hagelstein C et al (2016) Correlation of observed-to-expected MRI fetal lung volume and ultrasound lung-to-head ratio at different gestational times in fetuses with congenital diaphragmatic hernia. AJR Am J Roentgenol 206:856–866
58. Rypens F, Metens T, Rocourt N et al (2001) Fetal lung volume: estimation at MR imaging — initial results. Radiology 219:236–241
59. Meyers ML, Garcia JR, Blough KL et al (2018) Fetal lung volumes by MRI: normal weekly values from 18 through 38 weeks' gestation. AJR Am J Roentgenol 211:432–438
60. Ruano R, Lazar DA, Cass DL et al (2014) Fetal lung volume and quantification of liver herniation by magnetic resonance imaging in isolated congenital diaphragmatic hernia. Ultrasound Obstet Gynecol 43:662–669
61. Recio Rodriguez M, Martinez de Vega V, Cano Alonso R et al (2012) MR imaging of thoracic abnormalities in the fetus. Radiographics 32:E305–E321
62. Biyyam DR, Chapman T, Ferguson MR et al (2010) Congenital lung abnormalities: embryologic features, prenatal diagnosis, and postnatal radiologic–pathologic correlation. Radiographics 30: 1721–1738
63. Tramontana A, Hartmann B, Hafner E (2019) DiGeorge syndrome chromosome region deletion and duplication: prenatal genotype–phenotype variability in fetal ultrasound and MRI. Prenat Diagn 39: 1225–1234
64. Marini D, Xu J, Sun L et al (2020) Current and future role of fetal cardiovascular MRI in the setting of fetal cardiac interventions. Prenat Diagn 40:71–83
65. Brugger PC, Prayer D (2006) Fetal abdominal magnetic resonance imaging. Eur J Radiol 57:278–293
66. Veyrac C, Couture A, Saguintaah M, Baud C (2004) MRI of fetal GI tract abnormalities. Abdom Imaging 29:411–420
67. Duncan KR, Baker PN, Gowland PA et al (1997) Demonstration of changes in fetal liver erythropoiesis using echo-planar magnetic resonance imaging. Am J Phys 273:G965–G967
68. Witzani L, Brugger PC, Hormann M et al (2006) Normal renal development investigated with fetal MRI. Eur J Radiol 57:294–302
69. Guys JM, Borella F, Monfort G (1988) Ureteropelvic junction obstructions: prenatal diagnosis and neonatal surgery in 47 cases. J Pediatr Surg 23:156–158
70. Nemec U, Nemec SF, Krakow D et al (2011) The skeleton and musculature on foetal MRI. Insights Imaging 2:309–318
71. Victoria T, Epelman M, Coleman BG et al (2013) Low-dose fetal CT in the prenatal evaluation of skeletal dysplasias and other severe skeletal abnormalities. AJR Am J Roentgenol 200:989–1000
72. Victoria T, Epelman M, Bebbington M et al (2012) Low-dose fetal CT for evaluation of severe congenital skeletal anomalies: preliminary experience. Pediatr Radiol 42:S142–S149
73. Victoria T, Capilla E, Chauvin NA et al (2011) MR evaluation of fetal demise. Pediatr Radiol 41:884–889